

Contents lists available at ScienceDirect

Physica E: Low-dimensional Systems and Nanostructures

journal homepage: www.elsevier.com/locate/physe



Probing topology and symmetry in topological crystalline insulators with magnetism



H.A. Fertig^{a,*}, Sahinur Reja^{a,c}, Shixiong Zhang^a, Luis Brey^b

- ^a Department of Physics, Indiana University, Bloomington, IN 47405-7105, USA
- ^b Instituto de Ciencia de Materiales de Madrid, CSIC, 28049 Cantoblanco, Spain
- ^c School of Mathematics and Physics, The University of Queensland, Brisbane, Queensland 4072, Australia

ARTICLE INFO

Keywords: Magnetism Topology RKKY interactions

ABSTRACT

Topological crystalline insulators are classes of materials in which the electronic structure hosts non-trivial topology protected by some symmetry of the crystal. The paradigm of these are (Sn/Pb)Te alloys, for which the protection comes from mirror symmetry. The topology necessitates that gapless surface states are present for a bounded system even as the bulk is gapped. When magnetic dopants which are exchange-coupled to the electrons are added to the system, near the surface they may order. We demonstrate that the magnetic ordering at the surface reflects the symmetry of the bulk and leads to a rich set of possible ferromagnetic groundstates, with the particular form of this chosen out by the electron surface density, which in principle may be controlled by an external gate. The effective spin stiffness at the surface has an unusual "emergent" long-range form which follows from the Dirac nature of the electronic dispersion at the surface, with interesting consequences for the domain walls. Possible experimental signatures of this physics are discussed.

1. Introduction

Some of the most interesting developments in condensed matter physics in the last few decades have involved electronic systems in which topology plays a non-trivial role. The paradigm for this is the quantum Hall system [1], a two-dimensional electron gas subject to a perpendicular magnetic field. When this system is placed in a spatially periodic potential, an intricate band structure develops [2], and the Hall conductivity associated with these bands turns out to be a topological invariant [3], the Chern number. When this Chern number is different than zero the system supports a non-vanishing, quantized Hall conductivity [1], and for finite size systems there are robust gapless states at the edges [4] even as the bulk spectrum is gapped.

In recent years it has been recognized that the rich physics descending from non-trivial topology is not restricted to electrons in magnetic fields. In zero magnetic field there are now many examples of topological insulators and superconductors [5,6], both two and three dimensional. An important example of the three-dimensional case are topological crystalline insulators (TCI's) [7]. In these systems the gapless states at a sample boundary come in the form of Dirac cones [8], electronic states with a two-dimensional (surface) dispersion that varies linearly around a doubly-degenerate Dirac point. For TCI's this degeneracy is protected by a crystalline symmetry at one or more specific

points in the surface Brillouin zone. The breaking of this symmetry as the wavevector deviates from such points leads to level repulsion, causing the energy dispersion. The resulting gapless surface states invade the bulk gap, and when the system Fermi energy resides there, the surface states dominate its conduction properties. Such behavior is rather analogous to what occurs in the quantum Hall system [1].

A paradigm for TCI's that has been of great recent interest are (Pb,Sn)Te and related alloys [9-14]. In these systems the crystalline symmetries protecting the surface states are mirror reflections across high symmetry planes. When the crystal is cut in such a way that the surface leaves one or more of the mirror symmetries undisturbed, the surface can host gapless states. The symmetries, however, can be disturbed in more subtle ways [15,16], in particular by magnetic dopants. At long wavelengths the random placement of such impurities to a first approximation leaves the mirror symmetry intact; however, if they order magnetically, the resulting magnetization may align in such a way that mirror symmetry is broken. Qualitatively, one may expect such behavior should in fact be favorable: by forming such a gap, filled electron states are energetically pushed down, lowering the overall electronic energy of the system [17]. This is essentially a long-wavelength description of coupling between pairs of magnetic moments mediated by conduction electrons, resulting in the well-known "RKKY" interaction. While this has been thoroughly considered in the context of

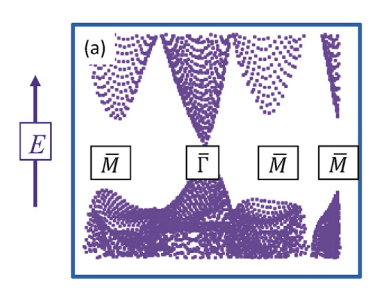
E-mail address: hfertig@indiana.edu (H.A. Fertig).

^{*} Corresponding author.

topological insulators protected by time-reversal symmetry [18–22], the resulting ordered groundstates turn out to be less rich than in the TCI case [23]: the former usually supports ferromagnetism moments perpendicular to the surface, or spin-glass states.

By contrast, in TCI systems the favored magnetization directions are not determined by the surface, but instead by the high symmetry directions of the bulk crystal lattice. This behavior is nicely illustrated when one considers a (111) surface of (Sn,Pb)Te [14,24-26]. This surface hosts four surface Dirac points in the surface Brillouin zone. Assuming the presence of substitutional isoelectronic magnetic impurities diluted into the system (or dopant magnetic impurities compensated by non-magnetic ones) the chemical potential may lie in the bulk gap. The absence of bulk conducting electrons implies the absence of substantial RKKY coupling there, and one expects the bulk moments to be disordered. The conducting surface states however do couple magnetic moments in their vicinity, leading to surface magnetism. The direction of lowest energy for the magnetization depends on which gap opening(s) of the various Dirac points dominates the total electronic energy. In turn this implies that favored magnetization directions will depend on the chemical potential μ . In principle this may be adjusted via a gate potential, leading to a possibly useful way to electrically control the magnetization direction.

Figs. 1 and 2 illustrate the physics, which is derived from a numerical tight-binding model representing a TCI slab with two open faces of (111) surfaces of (Pb,Sn)Te with magnetic moments embedded in them. Fig. 1 illustrates the total electronic energy of the system as a function of the magnetization orientation for two different chemical potentials μ , showing that the low energy orientations are sensitive to this parameter. Fig. 2 shows in more detail how this happens: the energies of surface electronic states penetrating the bulk gap, which would comprise four gapless Dirac cones in the absence of the magnetic moments, now have gaps, with relative sizes that depend on the magnetization orientation. The single particle energies are illustrated in a "flattened" manner, with the momentum (horizontal) axis along a particular direction in the surface Brillouin zone, and states at different momenta perpendicular to this direction all shown vertically above and below one another. The plot makes clear that the energy structure is quite sensitive to the magnetization orientation, which leads to very



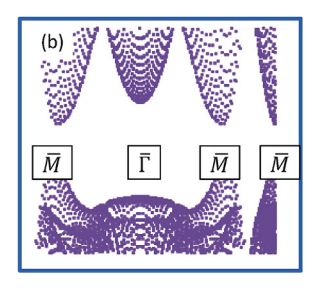


Fig. 2. Tight-binding energy levels near bulk gap energy for a slab geometry with magnetic moments near surfaces. In (a) the levels are shown for magnetization oriented along the bulk $\Gamma-L$ direction associated with a surface \overline{M} point. In (b) the orientation is along a bulk $\Gamma-L$ direction associated with the surface $\overline{\Gamma}$ point.

different minimal energy magnetization directions for different μ 's.

To understand these results in more detail, we next discuss the tightbinding model that underlies it.

2. From tight-binding to surface Hamiltonians

Figs. 1 and 2 are based on a tight-binding Hamiltonian for materials in the (Sn,Pb)Te class, which has a rocksalt structure. Its explicit form [9] is given by $H_{bulk} = H_m + H_{nn} + H_{nnn} + H_{so}$, with

$$H_{m} = \sum_{j} m_{j} \sum_{\mathbf{R},s} \overrightarrow{c}_{j,s}^{\dagger}(\mathbf{R}) \cdot \overrightarrow{c}_{j,s}(\mathbf{R}),$$

$$H_{nn} = t \sum_{(\mathbf{R},\mathbf{R}'),s} \overrightarrow{c}_{a,s}^{\dagger}(\mathbf{R}) \cdot \overrightarrow{d}_{\mathbf{R},\mathbf{R}'} \cdot \overrightarrow{d}_{\mathbf{R},\mathbf{R}'} \cdot \overrightarrow{c}_{b,s}(\mathbf{R}') + h. c. ,$$

$$H_{nnn} = \sum_{j} t'_{j} \sum_{((\mathbf{R},\mathbf{R}')),s} \overrightarrow{c}_{j,s}^{\dagger}(\mathbf{R}) \cdot \overrightarrow{d}_{\mathbf{R},\mathbf{R}'} \cdot \overrightarrow{d}_{\mathbf{R},\mathbf{R}'} \cdot \overrightarrow{c}_{j,s}(\mathbf{R}') + h. c. ,$$

$$H_{so} = i \sum_{j} \lambda_{j} \sum_{\mathbf{R},s,s'} \overrightarrow{c}_{j,s}^{\dagger}(\mathbf{R}) \times \overrightarrow{c}_{j,s'}(\mathbf{R}) \cdot (\overrightarrow{\sigma})_{s,s'}.$$

$$(1)$$

In these equations $\overrightarrow{\sigma}$ is the vector of Pauli matrices. **R** labels the sites of a cubic lattice, j=a,b are the species type (Sn/Pb or Te), with on-site energies $m_{a,b}$, and $s=\uparrow$, \downarrow is the electron spin. The vector operator $\overrightarrow{c}_{j,s}(\mathbf{R})$ annihilates electrons in p_x,p_y and p_z orbitals, and λ_j characterizes the strength of spin-orbit coupling in the system. The quantities $\overrightarrow{d}_{\mathbf{R},\mathbf{R}'}$ are unit vectors pointing from **R** to **R'**, and the sum over (**R**, **R'**) denotes

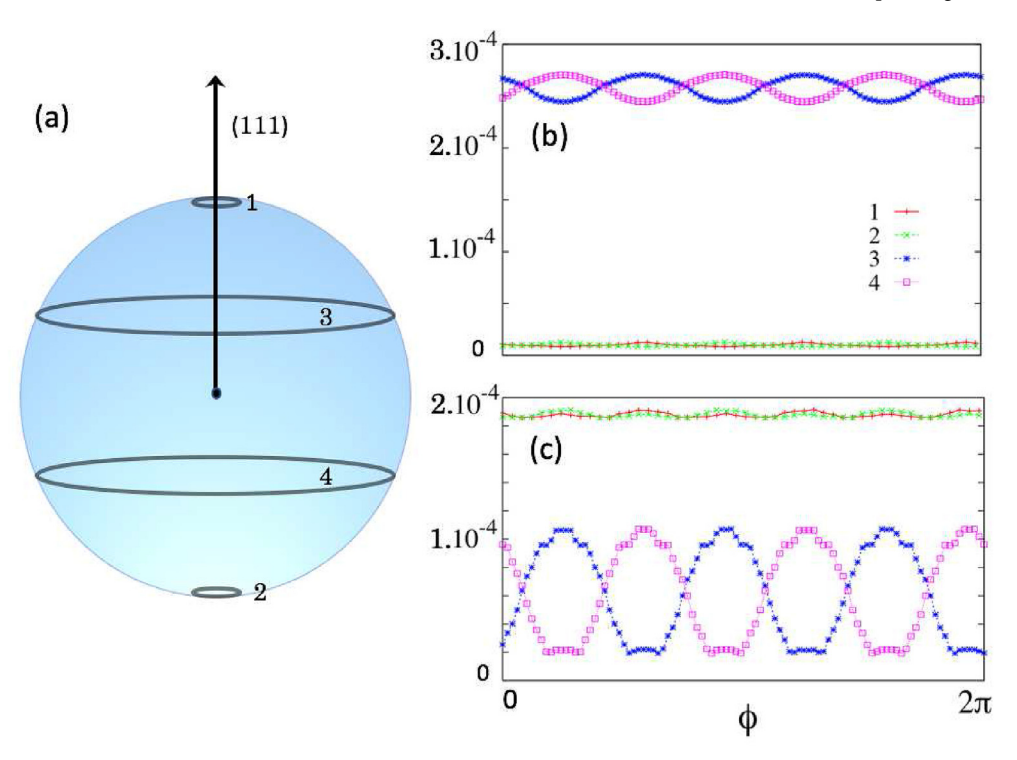


Fig. 1. Electronic energy for different magnetization orientations. (a) Representation of Bloch sphere, illustrating different possible orientations of the magnetization. Four labeled circles show different paths along which the system energy is shown in (b) and (c). (b) Total electron energy vs. magnetization orientation for chemical potential μ near E_{Γ} , as a function of azimuthal angle φ , for the four paths illustrated in (a). Paths 1 and 2 are lower in energy, illustrating that magnetization near the poles of the Bloch sphere are favored. (c) Total electron energy vs. magnetization orientation for chemical potential μ near $E_{\overline{M}}$, as a function of azimuthal angle φ , for the four paths illustrated in (a). Paths 3 and 4 are lower in energy, illustrating that magnetization directions closer to the equator are favored. Note there is a total of six minimal energy directions in this case.

positions which are nearest neighbors, while ((R, R')) denotes next nearest neighbors.

For appropriately chosen parameters, the model is a direct gap semiconductor with smallest gaps at the L $[\mathbf{k} = \mathbf{k}_1, \, \mathbf{k}_2, \, \mathbf{k}_3, \, \mathbf{k}_4 \equiv \left(\frac{\pi}{2}, \, \frac{\pi}{2}, \, \frac{\pi}{2}\right), \, \left(-\frac{\pi}{2}, \, \frac{\pi}{2}, \, \frac{\pi}{2}\right), \, \left(\frac{\pi}{2}, \, -\frac{\pi}{2}, \, \frac{\pi}{2}\right), \, \left(\frac{\pi}{2}, \, \frac{\pi}{2}, \, -\frac{\pi}{2}\right) \text{ in}$ units of the inverse nearest neighbor separation]. For k precisely at an L-point the nearest neighbor hopping integral vanishes so that the states at these points have well-defined sublattice index. Adjusting $m_b - m_a =$ m continuously allows two states to cross in energy, leading to band inversion and a transition from trivial to topological bands [9]. In practice, this parameter is adjusted in the real material by varying the relative densities of Pb and Sn in the alloy; in the virtual crystal approximation, this is taken into account by adjusting the electron potential at the site in the rocksalt structure where these atoms reside. Precisely at the m value for the topological transition, with k set to one of the *L*-points one encounters a four-fold degenerate manifold of states. The Hamiltonian may then be expanded for small deviations \mathbf{q} from an L-point to obtain an effective long-wavelength Hamiltonian [27]. For example, near the $k = k_1$ point one finds

$$\bar{H}_{1} = Aq_{3}\tau_{x} - B[q_{1}\tilde{\sigma}_{2} + q_{2}\tilde{\sigma}_{1}]\tau_{y} + [m + C_{12}^{(-)}(q_{1}^{2} + q_{2}^{2}) + C_{3}^{(-)}q_{3}^{2}]\tau_{z}
+ C_{12}^{(+)}(q_{1}^{2} + q_{2}^{2}) + C_{3}^{(+)}q_{3}^{2}.$$
(2)

In this expression, $\tilde{\sigma}_1 \equiv \frac{\sqrt{3}}{2} \sigma_x - \frac{1}{2} \sigma_y$ and $\tilde{\sigma}_2 \equiv \frac{\sqrt{3}}{2} \sigma_y + \frac{1}{2} \sigma_x$ are 2×2 matrices acting on the 1,2 indices of the basis states with different quantum numbers under three-fold rotations along the \hat{k}_1 direction, and τ_x , τ_y , τ_z are standard Pauli matrices acting on the sublattice index. The coefficients A, B, $C_{12}^{(\pm)}$ and $C_3^{(\pm)}$ may each be written explicitly in terms of the tight-binding parameters [27]. Finally, the wavevector coordinate q_3 represents the ${\bf q}$ component along the ${\bf k}_1$ direction, while q_1 and q_2 are components perpendicular to this. The matrix $\tilde{\sigma}_1$ in Eq. (2) carries out a mirror reflection which is a symmetry of H_{bulk} ; perturbations which do not spoil this symmetry will result in an effective Hamiltonian near an L point of a similar form [7]. Analogous approximate forms (H_{2-4}) for the other three L points can be obtained in similar ways.

We now specialize to the (111) surface of this system. The resulting system is two-dimensional, with a Brillouin zone in the form of a hexagon; in standard notation the central point of this is labeled $\bar{\Gamma}$ and the centers of the six edges are \bar{M} points. When the periodicity of the reciprocal lattice is taken into account, only three of the six \bar{M} points are distinguishable. If one projects the four bulk L points onto the surface, they coincide with the $\bar{\Gamma}$ point and the three \bar{M} points. This geometry is illustrated in Fig. 3. For m<0 the bands host nontrivial topology [9], protected in this system by mirror symmetries which the surface respects, so that it necessarily hosts gapless states [8]. Low energy forms of these may be explicitly constructed [23,28–30], and used to find surface Hamiltonians in the vicinity of the $\bar{\Gamma}$ and each of the \bar{M} points [23]. These take the form

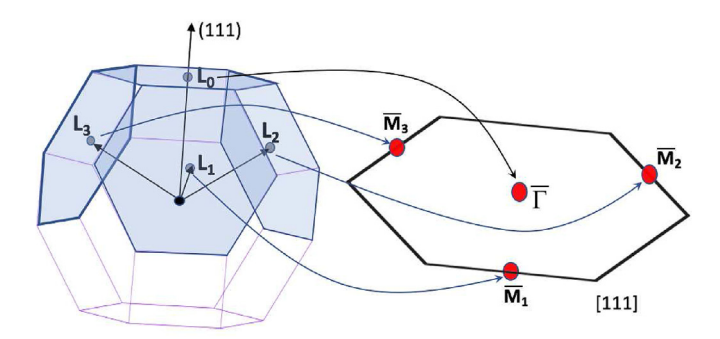


Fig. 3. Illustration of the bulk and surface Brillouin zones, showing how the various L points, labeled with subscripts 0–3 to distinguish them, map to the $\overline{\Gamma}$ and \overline{M} points. The latter are given subscripts 1–3 to emphasize the specific L points with which they are associated.

$$H_{\bar{\Gamma}} \equiv B[q_1 \tilde{\sigma}_2 + q_2 \tilde{\sigma}_1] + E_{\bar{\Gamma}} \tag{3}$$

and

$$H_{\bar{M}} \equiv \frac{AB}{\sqrt{A^2 + \eta^2 B^2}} [(\eta^2 - 1)q_2 \tilde{\sigma}_1 + q_1 \tilde{\sigma}_2] + E_{\bar{M}}. \tag{4}$$

Note that the states which the $\tilde{\sigma_i}$ operators act upon in $H_{\bar{M}}$ are different than those of $H_{\bar{\Gamma}}$. Analogous results may be obtained for the other two \bar{M} points by $2\pi/3$ rotations of Eq. (4).

3. Surface magnetism

Magnetic ions such a manganese diluted into (Pb,Sn)Te are known to typically enter substitutionally for the Sn/Pb atoms, and the coupling of the magnetic moments with the conduction electrons can be modeled rather well with an s-d model [31], $H_{sd}=J\sum_i \vec{S}(\mathbf{r}_i)\cdot \vec{s}_i$, where \vec{s}_i represents an impurity spin at location \mathbf{r}_i and $\vec{S}(\mathbf{r}_i)$ is the conduction electron spin density [32]. Since we are considering situations in which the chemical potential is in the bulk gap, there are effectively no carriers in the bulk of the system to couple these moments, and one expects them to be in a disordered state. This contrasts with the surface, for which gapless conduction electrons should couple impurity spins that happen to reside near the surface via the RKKY interaction. This overall situation suggests an appropriate model involves just the magnetic moments near the surface, residing on a single sublattice.

The calculations leading to Eqs. (3) and (4) involved computing explicit forms for the wavefunctions which were used to project the bulk Hamiltonian onto the surface, and these may be used to compute the contribution of H_{sd} to these effective Hamiltonians [27]. To further simplify the model, we assume the impurity spins ferromagnetically order and treat the Hamiltonian in mean-field theory; the linear stability of the state against formation of a spin-density wave can then be checked. The resulting effective Hamiltonian takes a generic form,

$$H_i \approx E_i + \alpha_i (q_2 - b_2) \widetilde{\sigma}_1 + \beta_i (q_1 - b_1) \widetilde{\sigma}_2 + \Delta_i \widetilde{\sigma}_3, \tag{5}$$

where i denotes either the $\overline{\Gamma}$ or one of the \overline{M} points, and $q_{1,2}$ represent wavevector components along the surface. (Note the relationships between (q_1, q_2) and (q_x, q_y, q_z) depend on the specific Dirac point i.) Because of the surface symmetry, $\alpha_{\Gamma} = \beta_{\Gamma}$, but $\alpha_{\overline{M}} \neq \beta_{\overline{M}}$. The offsets b_1 and b_2 are proportional to components of the impurity magnetization perpendicular to \mathbf{k}_i , while Δ_i is proportional to the component along it. Energy eigenvalues of 5 have the form $\epsilon_i = E_i \pm \sqrt{\alpha_i^2 (q_1 - b_1)^2 + \beta_i^2 (q_2 - b_2)^2 + \Delta_i^2}$. Importantly, when the magnetization aligns along a $\Gamma - L$ direction and $\mu \sim E_i$, a gap opens in the corresponding surface spectrum that lowers its contribution to the total electron energy [17]. This behavior is shown explicitly in Fig. 2, and is the driving physics behind the orientation dependences apparent in Fig. 1.

4. Tight-binding slab

These ideas may be checked numerically by computing the electronic energy of a system of electrons in the rocksalt structure with Hamiltonian described by H_{bulk} , but with open (111) surfaces, adding an effective magnetic field \overrightarrow{b} near the surface only on the a sublattice. Details of the calculation are presented in Ref. [27].

As a first pass at this, we first consider the system with a relatively small unit cell, which corresponds to a relatively large density of impurities. While this differs from the physical situation, it captures the correct qualitative physics, and allows us to study a wide enough slab that the surfaces are effectively decoupled. As anticipated, among the four the Dirac cones the one with largest magnetization projection along its corresponding Γ - L direction develops the largest gap. This is demonstrated explicitly in Fig. 2. Because states in the vicinity of $E_{\bar{\Gamma}}$ and $E_{\bar{M}}$ are repelled from the Dirac points by the magnetization, with

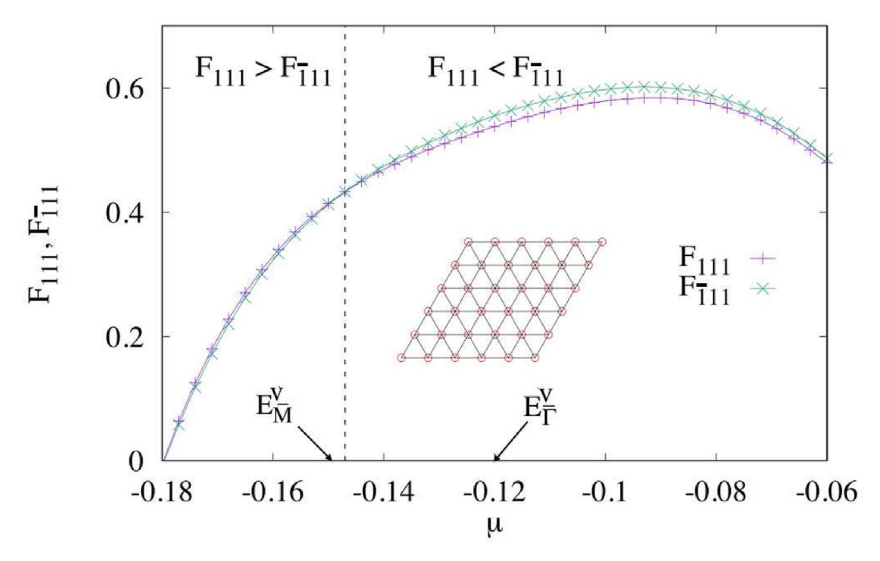


Fig. 4. Free energy per surface atom F_{111} and F_{111} in units of nearest neighbor hopping t, when magnetic moments are oriented in the (111) direction and in the ($\overline{1}11$) direction respectively, as a function of chemical potential, for $J[\vec{s}'] = 0.3$ in H_{sd} . (A straight line has been subtracted from these energies so that the two curves can be distinguished.) Dashed line illustrates regions where different orientations have lower energy. E_{Γ}^{V} and E_{M}^{W} indicate valence band tops when \vec{s} is oriented in each direction respectively. In these calculations there are 2 magnetic ions for 9 atoms on the surface, which is illustrated in the inset.

states raised and lowered by equal amounts, it is clear that the total electronic energy will be the most strongly lowered when the chemical potential μ is close to either of these two Dirac point energies. For fixed chemical potential, this means that when $\mu{\sim}E_{\Gamma}$, the energy is minimized when the magnetization is along the \hat{k}_1 direction, while for $\mu{\sim}E_{\bar{M}}$, it is minimized when the magnetization is along any of the $\hat{k}_{2,3,4}$ directions. The numerical results presented in Fig. 1 confirm these expectations. Thus in the $\mu{\sim}E_{\bar{\Gamma}}$ case one finds two (equal) energy minima on the Bloch sphere, while for $\mu{\sim}E_{\bar{M}}$ there are six.

To further substantiate this, we also examined a more dilute magnetic moment model, with impurities present for 2/9 of the atoms of one sublattice near the surface, with results shown in Fig. 4. The main panel shows the Gibbs free energies F_{111} and F_{111} of the system ($\langle H_{bulk} \rangle - \mu N$ with N the number of electrons) when the magnetic moments are oriented in the (111) direction and in the ($\overline{1}$ 11) directions, as a function of chemical potential. The results again demonstrate that energetically favored directions are determined by μ . One may also use this geometry to verify that orienting the two surface magnetic moments in different directions always raises the energy of the system, supporting our assumed ferromagnetic ordering, and that different placements of the impurities in the unit cell on one of the sublattices has little effect [23].

Because of the small lateral size of our unit cells, the numerical test of ferromagnetic ordering is limited to relatively short wavelengths. To test the stability of this ordering at long wavelengths, we can consider the change of energy in the system perturbatively. We do this with an effective field that varies spatially with some wavevector \overrightarrow{Q} , $b_{1,2}(\mathbf{r}) = b_{1,2}^{(0)} + \delta b_{1,2} \cos{(\mathbf{Q} \cdot \mathbf{r})}$, $\Delta(\mathbf{r}) \equiv \Delta^{(0)} + \delta \Delta \cos{(\mathbf{Q} \cdot \mathbf{r})}$. To compute the change in energy we adopt as our basic Hamiltonian Eq. (5), assuming for simplicity $a_i = \beta_i \equiv a$, use the directions associated with q_1 and q_2 to define x and y directions on the surface, and compute the change in energy to second order in $\delta b_{1,2}$, $\delta \Delta$, and Q. The calculation yields a correction of the form [27].

$$\frac{\delta E(Q) - \delta E(0)}{S} = \frac{1}{2} \sum_{\mu,\nu = x,y} \rho_{\mu,\nu} Q_{\mu} Q_{\nu}, \tag{6}$$

where the coefficients $\rho_{\mu,\nu}$ are all second order in the deviations $\delta b_{1,2}$, $\delta \Delta$, and the eigenvalues of the 2 × 2 matrix it represents are positive. This demonstrates that if the effective field from the surface magnetization has a spatial oscillation, the resulting energy increases with increasing oscillation wavevector, as should be for a ferromagnetically

aligned groundstate. The stiffnesses $\rho_{\mu,\nu}$ have the surprising property that they diverge as $1/\Delta^{(0)}$ [27], which suggests that as the magnetization density gets small, the system becomes very stiff. This unintuitive result is unique to this system, and suggests that surface magnetism in this system should have some unusual properties. We next turn to a discussion of these.

5. Discussion

We now turn to physical consequences of the surface magnetism discussed above, focusing on temperature ranges where the impurity magnetic moments may be treated classically. One behavior with possible utility in spintronic devices is the connection between the surface electron density and magnetization direction: a small change in the chemical potential near the surface will cause the spins to change from orienting along the normal to the surface to a nearly planar direction. This means that the magnetic state can be controlled by an electric gate potential.

Beyond this, the observation that $\rho_{\mu\nu}\sim 1/\Delta^{(0)}$ has a number of consequences. For fixed μ , the existence of multiple groundstate directions implies that there should be domain wall (DW) excitations in the system, with energy per unit length scaling as $\sqrt{\Delta^{(0)}\rho_0}$, with ρ_0 an effective average stiffness. Naïvely this remains finite even as $\Delta^{(0)}$ vanishes, as should happen at high enough temperature where the magnetism disorders. In fact one does not expect the stiffness to truly diverge as the magnetically induced gap is closed due to thermal fluctuations. This stems from the fact that Fermi surface of the surface electrons becomes smeared at finite temperature, eradicating the effect of the gap closing.

The divergent behavior of the stiffness at zero temperature may be understood in terms of the pairwise RKKY interaction between spins when the exchange interaction is mediated by Dirac electrons with chemical potential precisely located at the Dirac point: this interaction falls off as $1/R^3$ [33]. This is a long-range interaction which for collection of spins leads to spin *gradient* interactions that fall off only as 1/R, an effective three-dimensional Coulomb interaction. The gap opening cuts off this interaction and induces an effective screening length, so that one can model the interactions among gradients as having a $e^{-\xi R}/R$, with $\xi \sim v_F/\Delta_0$ and v_F the electron Fermi velocity. At temperatures T where Δ_0 is small on average, this length scale can be replaced by $\xi \sim v_F/k_BT$ [34]. In particular this means that upon

approaching the thermal disordering phase transition, the effective stiffness does not diverge, but rather remains finite at a scale set by the temperature. The long-range form of the gradient interactions is *emergent*, in the sense that it will present itself when the magnetization is small even at low temperature. This should be the case when the impurity density n_{imp} is small. Counter-intuitively, the number of spins coupled together (i.e., within a range of order ξ) in an ordered phase *diverges* as $n_{imp} \rightarrow 0$.

The unusual behavior of the stiffness makes itself felt most directly in how the transition temperature scales with n_{imp} . In both the six-state case [Fig. 1(c)] and in the Ising case [Fig. 1(b)], thermal disordering can be understood as a DW proliferation transition [35,36]. In either of these the transition temperature is proportional to the effective exchange stiffness at long wavelengths – $k_BT_c\sim J_{eff}$ – and because this stiffness is an interaction effect, one expects $J_{eff} \sim n_{imp}^2$ when the correlation length exceeds the average distance between impurities. The explicit presence of temperature in the effective screening length ξ changes this scaling to a T_c that instead varies linearly with n_{imp} . Note this means one expects the scaling of T_c with n_{imp} to differ for cases in which μ passes through a Dirac point from ones in which it does not: in the latter, the interaction is finite in range, with length scale $\xi \sim \pi/k_F$, where k_F is the Fermi wavelength ($v_F k_F = \mu$). Note also that the universality classes for thermal disordering in the Ising and six-state cases should be different: while the former is clearly in the Ising class, the latter transition is known to be in the Kosterlitz-Thouless universality class [36]. Thus we see that simply by adjusting the surface electron density, a rather rich variety of behaviors should be observable in the thermodynamics that the surface magnetism presents.

There are further special properties associated with DW's in this system. Because of the topological nature of the electron system, they host states that invade the magnetization-induced gaps [37,38]. At the critical temperature T_c where the transition occurs, one expects DW's to proliferate, opening a channel for conduction which is absent below T_c . This should lead to singular behavior in the surface conductivity that reflects the nature of the DW proliferation transition [39,40]. Moreover, one might detect the opening of such a conduction channel when it is probed via tunneling. A further possibility is to look for differences in surface conduction when the system is field-cooled through its critical temperature from when it is zero field-cooled. The latter leads to nucleation of groundstate domains with random orientation, and DW's between them which cannot relax on the time scale of an experiment. Thus one expects stronger surface conduction from a zero field-cooled sample [41–43].

In summary, the surface of a magnetically-doped TCI hosts magnetic ordering in the topological state even when the bulk is magnetically disordered. The unique electronic structure of a TCI surface leads to a rich set of possible ordered states, with defect structures – domain walls – that reflect how the symmetry of a surface is realized at the chemical potential of the conducting surface electrons. This allows thermal disordering transitions of a number of different universality classes to be realized in this single system, simply by adjusting the electron doping near the surface. In this way the magnetically-doped TCI system allows for an exploration of a diverse set of effective magnetic systems, all in a single setting.

Acknowledgements

The authors thank Fernando de Juan for helpful comments, and U. Nitzsche for technical assistance. This work was supported by the NSF through Grant Nos. DMR-1914451, DMR-1506263 and DMR-1506460, by the US-Israel Binational Science Foundation, by MEyC-Spain under grant FIS2015-64654-P, and by the ARC under the grant number DP180101483. Computations were carried out on the ITF/IFW and IU Karst clusters.

References

- T. Chakraborty, P. Pietiliainen, The Quantum Hall Effects, Fractional and Integral, second ed., Springer, 1995.
- [2] D.R. Hofstadter, Phys. Rev. B 14 (1976) 2239–2249 doi:10.1103/ PhysRevB.14.2239 https://link.aps.org/doi/10.1103/PhysRevB.14.2239.
- [3] D.J. Thouless, M. Kohmoto, M.P. Nightingale, M. den Nijs, Phys. Rev. Lett. 49 (1982) 405–408 doi:10.1103/PhysRevLett.49.405 https://link.aps.org/doi/10. 1103/PhysRevLett.49.405.
- [4] B.I. Halperin, Phys. Rev. B 25 (1982) 2185–2190 doi:10.1103/PhysRevB.25.2185 https://link.aps.org/doi/10.1103/PhysRevB.25.2185.
- [5] M.Ž. Hasan, C.L. Kane, Rev. Mod. Phys. 82 (2010) 3045–3067 doi:10.1103/ RevModPhys.82.3045 https://link.aps.org/doi/10.1103/RevModPhys.82.3045.
- [6] X.-L. Qi, S.-C. Zhang, Rev. Mod. Phys. 83 (2011) 1057–1110 doi:10.1103/ RevModPhys.83.1057 https://link.aps.org/doi/10.1103/RevModPhys.83.1057.
- [7] L. Fu, Phys. Rev. Lett. 106 (2011) 106802.
- [8] J. Liu, W. Duan, L. Fu, Phys. Rev. B 88 (2013) 241303(R).
- 9] T. Hsieh, H. Lin, J. Liu, W. Duan, L. Fu, Nat. Commun. 3 (2012) 982.
- [10] Y. Tanaka, et al., Nat. Phys. 8 (2012) 800.
- [11] S. Xu, et al., Nat. Phys. 3 (2012) 1192.
- [12] P. Dziawa, et al., Nat. Commun. 11 (2012) 1023.
- [13] Y. Okada, et al., Science 341 (2013) 6153.
- [14] C. Yan, et al., Phys. Rev. Lett. 112 (2014) 186801.
- [15] F. Zhang, X. Li, J. Feng, C. Kane, E. Mele, ???? ArXiv:1309.7682.
- [16] C. Fang, M.J. Gilbert, B.A. Bernevig, Phys. Rev. Lett. 112 (2014) 046801 doi:10.1103/PhysRevLett.112.046801 https://link.aps.org/doi/10.1103/ PhysRevLett.112.046801.
- [17] D. Efimkin, V. Galitski, Phys. Rev. B 89 (2014) 115431.
- [18] A. Liu, C. Liu, C. Xu, X. Qu, S. Zhang, Phys. Rev. Lett. 102 (2009) 156603.
- [19] R.R. Biswas, A.V. Balatsky, Phys. Rev. B 81 (2010) 233405 doi:10.1103/ PhysRevB.81.233405 http://link.aps.org/doi/10.1103/PhysRevB.81.233405.
- [20] I. Garate, M. Franz, Phys. Rev. B 81 (2010) 172408 doi:10.1103/ PhysRevB.81.172408 http://link.aps.org/doi/10.1103/PhysRevB.81.172408.
- [21] D. Abanin, D. Pesin, Phys. Rev. Lett. 106 (2011) 136802.
- [22] C.-X. Liu, B. Roy, J.D. Sau, Phys. Rev. B 94 (2016) 235421 doi:10.1103/ PhysRevB.94.235421 http://link.aps.org/doi/10.1103/PhysRevB.94.235421.
- [23] S. Reja, H. Fertig, L. Brey, S. Zhang, Phys. Rev. B 96 (2017) 201111 (R).
- [24] Z. Li, S. Shao, N. Li, K. McCall, J. Wang, S.X. Zhang, Nano Lett. 13 (2013) 5443–5448
- [25] A.A. Taskin, F. Yang, S. Sasaki, K. Segawa, Y. Ando, Phys. Rev. B 89 (2014) 121302 doi:10.1103/PhysRevB.89.121302 http://link.aps.org/doi/10.1103/PhysRevB.89. 121302.
- [26] J. Shen, Y. Jung, A.S. Disa, F.J. Walker, C.H. Ahn, J.J. Cha, Nano Lett. 14 (2014) 4183–4188.
- [27] S. Reja, H. Fertig, S. Zhang, L. Brey, L. Brink, M. Gunn, J.V. José, J.M. Kosterlitz, K.K. Phua (Eds.), Topological Phase Transitions and New Developments, World Scientific, 2018, https://doi.org/10.1142/11016 https://www.worldscientific. com/doi/abs/10.1142/11016.
- [28] C.-X. Liu, X.-L. Qi, H. Zhang, X. Dai, Z. Fang, S.-C. Zhang, Phys. Rev. B 82 (2010) 045122 doi:10.1103/PhysRevB.82.045122 https://link.aps.org/doi/10.1103/PhysRevB.82.045122.
- [29] P.G. Silvestrov, P.W. Brouwer, E.G. Mishchenko, Phys. Rev. B 86 (2012) 075302 doi:10.1103/PhysRevB.86.075302 http://link.aps.org/doi/10.1103/PhysRevB.86. 075302.
- [30] L. Brey, H.A. Fertig, Phys. Rev. B 89 (2014) 084305.
- [31] T. Dietl, C. Śliwa, G. Bauer, H. Pascher, Phys. Rev. B 49 (1994) 2230–2233 doi:10.1103/PhysRevB.49.2230 http://link.aps.org/doi/10.1103/PhysRevB.49. 2230.
- [32] J. Liu, C. Fang, L. Fu, arXiv:1604.03947 (2016).
- [33] L. Brey, H.A. Fertig, S. Das Sarma, Phys. Rev. Lett. 99 (2007) 116802 doi:10.1103/ PhysRevLett.99.116802 http://link.aps.org/doi/10.1103/PhysRevLett.99.116802.
- [34] T. Vojta, K. Hoffmann, M. Schreiber (Ed.), Computational Statistical Physics, Springer-Verlag, Berlin, 2002.
- [35] R. Shankar, Quantum Field Theory and Condensed Matter: an Introduction, Cambridge University Press, 2017.
- [36] J.V. José, L.P. Kadanoff, S. Kirkpatrick, D.R. Nelson, Phys. Rev. B 16 (1977) 1217–1241 doi:10.1103/PhysRevB.16.1217 http://link.aps.org/doi/10.1103/ PhysRevB.16.1217.
- [37] R. Jackiw, C. Rebbi, Phys. Rev. D 13 (1976) 3398.
- [38] A. Schaakel, Boulevard of Broken Symmetries, World Scientific, 2008.
- [39] T. Jungwirth, A.H. MacDonald, Phys. Rev. Lett. 87 (2001) 216801 doi:10.1103/ PhysRevLett.87.216801 http://link.aps.org/doi/10.1103/PhysRevLett.87.216801.
- [40] K. Dhochak, E. Shimshoni, E. Berg, Phys. Rev. B 91 (2015) 165107 doi:10.1103/ PhysRevB.91.165107 http://link.aps.org/doi/10.1103/PhysRevB.91.165107.
- [41] B.A. Assaf, F. Katmis, P. Wei, C.-Z. Chang, B. Satpati, J.S. Moodera, D. Heiman, Phys. Rev. B 91 (2015) 195310 doi:10.1103/PhysRevB.91.195310 http://link.aps. org/doi/10.1103/PhysRevB.91.195310.
- [42] K. Ueda, J. Fujioka, B.-J. Yang, J. Shiogai, A. Tsukazaki, S. Nakamura, S. Awaji, N. Nagaosa, Y. Tokura, Phys. Rev. Lett. 115 (2015) 056402 doi:10.1103/PhysRevLett.115.056402 http://link.aps.org/doi/10.1103/PhysRevLett.115.056402
- [43] Z. Tian, et al., Nat. Phys. 12 (2016) 134-138.